Seismic structure-soil-structure interaction between pairs of adjacent building structures

Knappett, Jonathan; Madden, P.; Caucis, K.

Published in:
Géotechnique

DOI:
10.1680/geot.SIP.14.P.059

Publication date:
2015

Document Version
Publisher's PDF, also known as Version of record

Knappett, J. A. *et al. Géotechnique* [http://dx.doi.org/10.1680/geot.SIP.14.P.059]

Seismic structure–soil–structure interaction between pairs of adjacent building structures

J. A. KNAPPETT*, P. MADDEN* and K. CAUCIS†

Structure–soil–structure interaction between adjacent structures, which may occur in densely populated urban areas, has received little attention compared to the soil–structure interaction of single isolated structures. Additionally, recent earthquakes in/near such areas (e.g. the Christchurch series, 2010–2011) have shown that large motions can be followed by strong aftershocks. In this paper, the seismic behaviour of isolated structures and pairs of adjacent structures under a sequence of strong ground motions has been investigated using a combination of centrifuge and finite-element modelling. The latter utilised an advanced constitutive model that can be parameterised from routine test data, making it suitable for use in routine design. The finite-element models were shown to accurately simulate the centrifuge-measured response (in terms of surface ground motion and structural sway, settlement and rotation) even after multiple strong aftershocks, so long as the buildings' initial conditions were reproduced accurately. For the case of a building structure with a close neighbour, structural drift and co-seismic settlement could be reduced or increased as a result of structure–soil–structure interaction, depending chiefly on the properties of the adjacent structure. This suggests that careful arrangement of adjacent structures and specification of their properties could be used to control the effects of structure–soil–structure interaction. In all cases where adjacent structures were present, permanent rotation (structural tilt) was observed to increase significantly, demonstrating the importance of considering structure–soil–structure interaction in assessing the seismic performance of structures.

KEYWORDS: centrifuge modelling; earthquakes; numerical modelling; sands

INTRODUCTION

Current seismic design of building structures considers the response of a building in isolation from its neighbours. Many of the most damaging earthquakes over the last 20 years, however, have struck heavily populated and highly urbanised areas, including those in Kobe (1995), Kocaeli (1999), Athens (1999), Wenchuan (2008) and the Christchurch series (2010–2011). Although damage may be expected to be high in these areas as there are many more 'targets' for the earthquake, the close spacing of the building stock will result in interaction between adjacent structures through the ground, a phenomenon which is here termed structure–soil–structure interaction (SSSI). There have been few previous attempts to study SSSI and these have often been highly simplified; however, it may be expected that, depending on the layout of adjacent buildings and their relative dynamic properties, the effects of SSSI may have either a beneficial or detrimental effect on the overall response of the structures, through changes in the local soil–structure interaction.

Previous studies of SSSI have generally focused on understanding changes in dynamic characteristics of adjacent rigid blocks (e.g. Tsogka & Wirgin, 2003) or simple oscillators (Alexander *et al.*, 2013), in each case on a linear elastic medium as a representation of the soil. Both shallow (Betti, 1997) and deep foundations (Padrón *et al.*, 2009) have previously been considered. Although these studies have provided useful information in terms of changes in fundamental periods of vibration and elastic spectral response, they are limited in that the soil–structure interaction is always linear elastic. This may be an acceptable assumption in a very small earthquake, but when the ground motions become large (such as in the strong recent earthquakes mentioned previously) the soil would be expected to be highly non-linear with significant plastic strains. Under these circumstances, not only would the effects of the SSSI on the dynamic structural response (e.g. inter-storey drift or spectral acceleration) be expected to change, but there may also be significant permanent settlement and rotation of the structures, which could be as damaging as the structural motions.

The ability to capture the permanent behaviour is particularly important considering that many of the earthquakes mentioned previously were associated with strong aftershocks, the most notable recent example being the Darfield (2010) and Christchurch (2011) earthquakes, which occurred less than 6 months apart, that is, before a substantial amount of repair could be conducted on damaged structures following the first earthquake. Permanent soil deformations will change the behaviour of the underlying soil. Settlement may lead to soil stiffening as a result of densification, making it potentially better able to transmit ground motions into the structure (and thereby potentially increasing the structural response). A bias in permanent rotation may be amplified in subsequent earthquakes owing to P–Δ effects. Current linear elastic approaches cannot incorporate such effects.

This paper, therefore, aims to study SSSI utilising methods that can incorporate non-linear elasto-plastic soil behaviour. First, dynamic centrifuge modelling is used to create a database of physical test data of pairs of adjacent low-rise simple structures having shallow foundations on sand, considering situations (*a*) where the structures have similar properties and (*b*) where the properties are dissimilar. Tests of the structures in isolation are also performed for comparison. In all cases, series of strong motions are applied to the models as an idealised representation of a sequence of

Manuscript received 4 April 2014; revised manuscript accepted 10 February 2015.
Discussion on this paper is welcomed by the editor.
* University of Dundee, Dundee, UK.
† Arup, Edinburgh, UK; formerly University of Dundee, Dundee, UK.

strong aftershocks. Non-linear finite-element modelling is then used to simulate these tests and is validated against the centrifuge test data. This will utilise the constitutive modelling approach outlined in Al-Defae *et al.* (2013), which was shown to closely simulate the dynamic constitutive behaviour of soil identical to that used herein at similar relative density in sequences of strong earthquakes for slope models atop a level bearing layer. The influence of modelling assumptions will also be discussed. Finally, the finite-element approach is used to gain insight into the influence of building arrangement and aftershocks on the seismic response of pairs of adjacent structures.

CENTRIFUGE MODELLING

All of the tests were conducted using a model scale of 1:50 and tested at 50***g*** using the 3·5 m radius beam centrifuge at University of Dundee, UK. All subsequent parameters are given at prototype scale, unless otherwise stated. Scaling factors for centrifuge modelling can be found in Muir Wood (2004).

Model structures

Two different structural models were produced that were designed to represent some of the key characteristics of low-rise buildings. Such buildings will generally form a much larger proportion of the building stock within an urban area compared to high-value, high-rise structures and are also less likely to have undergone detailed seismic design. They may therefore be more vulnerable and contribute more significantly to the overall cost of seismic damage following a major earthquake.

Each structure was modelled as a single-bay, single-degree-of-freedom (SDOF) sway frame on separated strip foundations, 100 mm long and 40 mm wide at model scale (5 m $\times$ $B = 2$ m at prototype scale). Steel mass plates were used to represent the dynamic mass of the structure, and vertical aluminium alloy plates, the same length as the foundations, were used to represent the sway stiffness of the structures (that would be provided by the columns). The centre-to-centre spacing between the foundations (s) was kept the same between the models, but the height was varied to change the position of the centre of mass above the soil surface and therefore alter the proportion of rocking to sway deformation between the two structures. The model structures are shown in elevation with model scale dimensions (in mm) in Fig. 1. The fundamental natural period (T_{n0}) of a building structure is typically related to its height, with taller buildings being laterally more flexible per unit mass and hence having higher T_{n0} (e.g. Goel & Chopra, 1997; BSI, 2005). To design the model structures, the relationship given in Eurocode 8 (BSI, 2005) was used for building structures less than 40 m high

$$T_{n0} = C_t H^{0·75} \tag{1}$$

where H is the overall height of the building and $C_t = 0·085$ (as an approximation for a steel moment resisting frame (MRF)). In each case, the structures are assumed to be SDOF idealisations of multi-storey structures that have a uniform distribution of mass and stiffness with height. The centre of mass of such structures would be approximately at the mid-height, and so in order to ensure the correct amount of overturning moment for a given value of H, the structure with the shorter period (hereafter termed 'short structure') represents a prototype structure $H = 6$ m high (centre of mass 3 m above founding plane). The structure with the longer period (hereafter termed 'long structure') represents a structure $H = 15$ m high (centre of mass 7·5 m above the founding plane). From equation (1), $T_{n0} = 0·33$ s and 0·65 s for the 'short' and 'long' period structures, respectively. The characteristics of the models are compared to the measured properties of a variety of real structures (after Goel & Chopra (1997) and Stewart *et al.* (1999)) in Fig. 2.

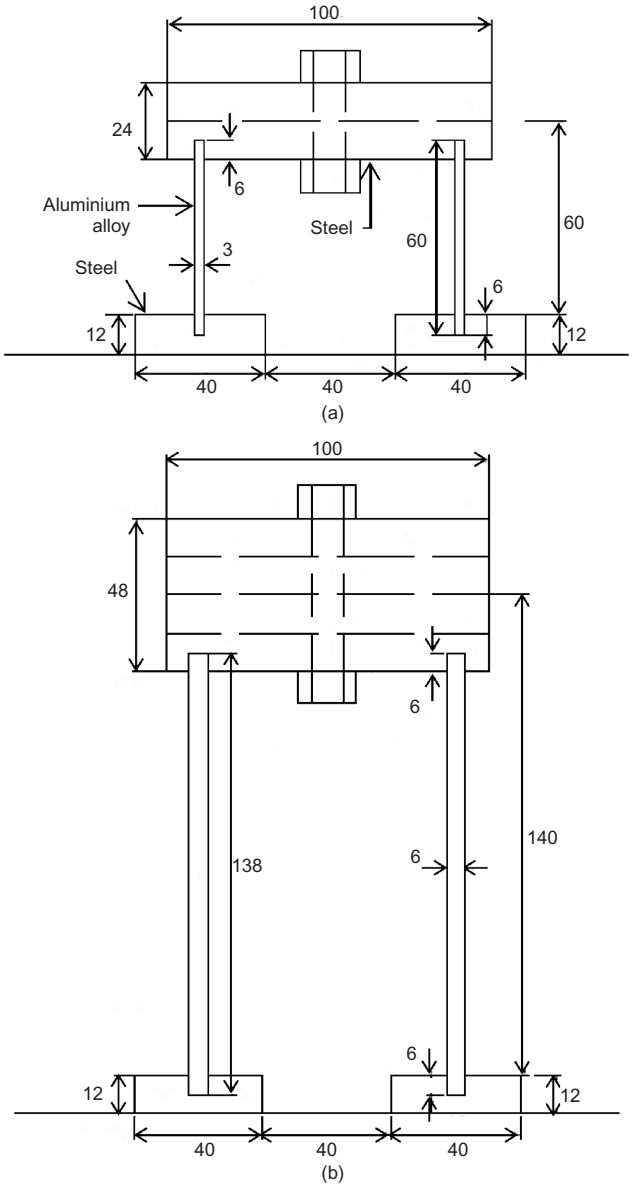

Fig. 1. Single-degree-of-freedom model structures: (a) 'short' period structure; (b) 'long' period structure. All dimensions at model scale in mm

The supported mass and stiffness of the plates representing the columns were then selected to match these values of T_{n0}. The mass at the top of each structure (M_{eq}) was selected first, which fixed the value of the bearing pressure (q) for a given static factor of safety (FS_v). The thickness of the vertical plates was then selected to provide a bending stiffness, EI (and therefore lateral sway stiffness, K_{eq}) such that the required T_{n0} was achieved for the mass selected, using

$$T_{n0} = 2\pi\sqrt{\frac{M_{eq}}{K_{eq}}} \tag{2}$$

A summary of the properties of the two structures at prototype scale is provided in Table 1. This table includes an estimate of FS_v when surface bearing on a uniform

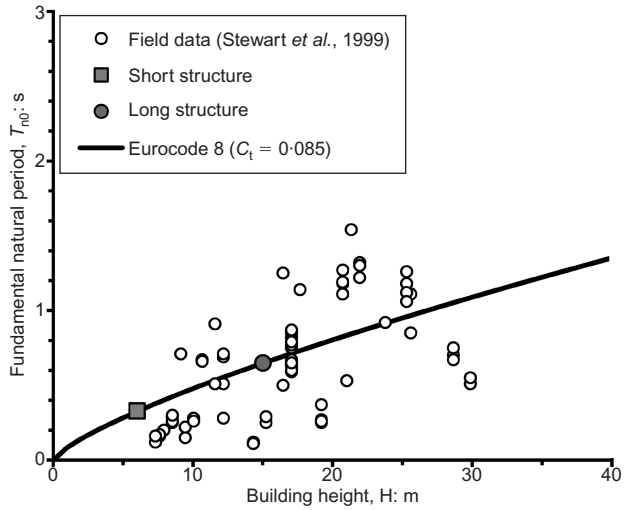

Fig. 2. Fundamental period of model structures and comparison to field data

Table 1. Properties of model structures (prototype scale)

Parameter: units	'Short' structure	'Long' structure
Total height, H: m	6	15
Height to C-of-M: m	3	7·5
Natural period, T_{n0}: s	0·33	0·65
Bearing pressure, q: kPa	161	276
Static factor of safety, FS_v	9·5	5·5
M_{eq}: t	235	469
K_{eq}: MN/m	87·2	44·1
Vertical plate EI: MN m^2/m	19·6	155·1
Footing spacing, s: m	4	4

deposit of dry sand as used in the centrifuge tests (relative density $D_r = 58\%$, unit weight $\gamma = 16{\cdot}2\,\text{kN/m}^3$ and peak friction angle $\phi'_p = 40°$), which was determined using

$$FS_v = \frac{0{\cdot}5\gamma B s_\gamma N_\gamma}{q} \tag{3}$$

In determining FS_v, N_γ and s_γ were calculated for $\phi'_p = 40°$ following Salgado (2008) and Lyamin *et al.* (2007), respectively, although it should be noted that almost identical values are found using the relationships provided in Eurocode 7 (BSI, 2004). The same foundation type and size was used for both structures, which resulted in a higher value of FS_v for the short structure due to its lower applied bearing pressure.

These model structures were used in a total of seven centrifuge tests. Two of these, PM003 and PM004, tested the single structures in isolation (ground properties are described in the following section). Tests PM005 and PM006 tested the same adjacent pair of two long structures, but with different edge-to-edge (inter-building) spacing between the structures; PM008 was comparable to PM006 in terms of spacing, but tested the two short structures as an adjacent pair. Finally, tests PM009 and PM011 tested pairs of one short and one long structure; by reversing the order of the structures in the box, the effect of earthquake direction relative to the arrangement of structures could be considered, as the ground motions were always applied in the same direction. Spacing between structures in the adjacent cases was kept to a minimum to consider the condition where SSSI effects will likely be most significant (assuming that these reduce as spacing increases). A summary of the test configurations is given in Table 2.

Model preparation and soil properties

As the tests reported here focus on the effects of structural properties and arrangement on SSSI, a single set of soil properties was used in all of the tests. Dry HST95 Congleton silica sand was air-pluviated into an equivalent shear beam (ESB) container to a target relative density of $D_r = 55$–60% (the range accounts for the accuracy with which this property can be replicated and measured within a model soil bed) to produce a uniform layer with a prototype thickness of 10 m. The measured relative density achieved in each test is shown in Table 2. The design and performance of the ESB container is described by Bertalot (2012) and the basic soil properties for HST95 are given in Table 3 after Lauder (2011). As the rigid base of the container lay below the layer of sand, the ground profile represents ground type E according to Eurocode 8 (BSI, 2005).

During pluviation, the soil was instrumented with type ADXL78 MEMS accelerometers ($\pm 70\boldsymbol{g}$ range) manufactured by Analog Devices, as shown in Fig. 3 (PM003 and PM006 are shown as examples). These were used to measure the input motion (point E), free-field ground motion 1 m below the ground surface (point F) and accelerations beneath (D) and between (G) the structures at the same depth as the

Table 3. State-independent physical properties of HST95 silica sand (after Lauder, 2011)

Property	Value
Specific gravity, G_s	2·63
D_{10}: mm	0·09
D_{30}: mm	0·12
D_{60}: mm	0·17
C_u	1·9
C_z	1·06
Maximum void ratio, e_{max}	0·769
Minimum void ratio, e_{min}	0·467

Table 2. Centrifuge testing programme

Test ID	Configuration	Structure type (left)	Structure type (right)	Inter-building spacing: m	Relative density: %
PM003	Isolated	Short		N/A	58
PM004	Isolated	Long		N/A	59
PM005	Adjacent, similar	Long	Long	2	57
PM006	Adjacent, similar	Long	Long	1	58
PM008	Adjacent, similar	Short	Short	1	58
PM009	Adjacent, dissimilar	Long	Short	1	59
PM011	Adjacent, dissimilar	Short	Long	1	56

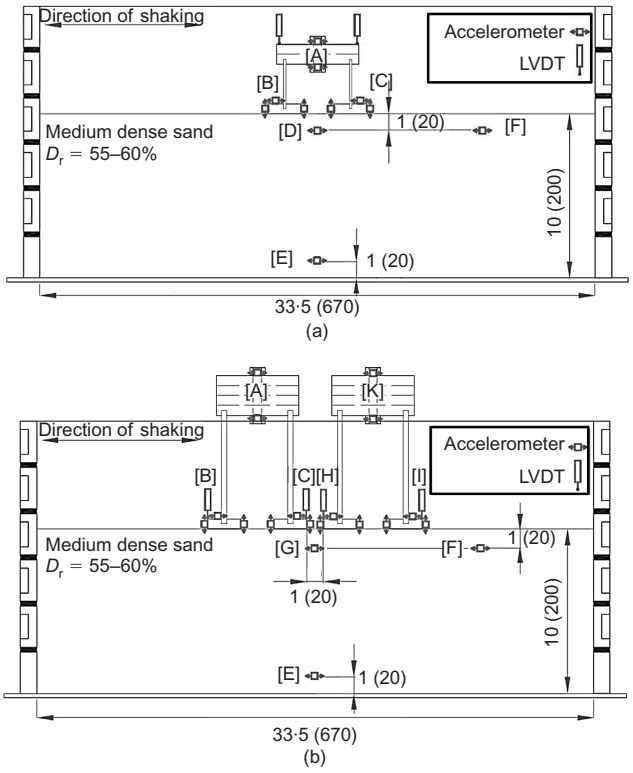

Fig. 3. Layout of centrifuge tests: (a) isolated structure case (PM003 shown); (b) adjacent structure case (PM006 shown). All dimensions at prototype scale in m (model scale in mm)

free-field instrument, to examine near-field effects of SSSI on the ground motion. Identical accelerometers were also attached to the structures, as shown in Fig. 3. These were used to measure the dynamic motion of the foundations and equivalent mass. Through high-pass filtering and integration, the dynamic displacements were determined at these locations with rotational bias removed, and the difference between them represented the dynamic inter-storey drift.

The container and model soil beds were loaded onto the centrifuge and the structures were placed on the surface after loading using a post-level to place them as accurately as possible. In all cases the structures occupied a maximum of the central 33% of the ESB (Fig. 3(b)) to minimise any potential boundary effects within the container. An overhead gantry was then placed above the structures allowing linear variable differential transformers (LVDTs) to be placed as shown in Fig. 3 to measure average settlement and global rotation (tilt) of the structures. During spin-up of the centrifuge the response of the LVDTs was recorded such that the initial settlement and tilt of the structures, prior to earthquake shaking, were known. These initial conditions are presented in Fig. 4.

Dynamic excitation

Following spin-up, a sequence of strong ground motions was applied to each of the models using the Actidyn QS67-2 servo-hydraulic earthquake simulator (EQS), the performance of which is detailed in Bertalot *et al.* (2012) and Brennan *et al.* (2014). In each case, a horizontal motion recorded at the Nishi-Akashi recording station in the $M_w = 6{\cdot}9$ Kobe earthquake (1995) was used. This record was downloaded from the PEER (Pacific Earthquake Engineering Research) NGA database and, unscaled, had a peak acceleration of $a_g = 0{\cdot}43\boldsymbol{g}$. For the purpose of these tests, the motion was rescaled to $0{\cdot}1\boldsymbol{g}$ and $0{\cdot}5\boldsymbol{g}$ nominal peak accelerations and

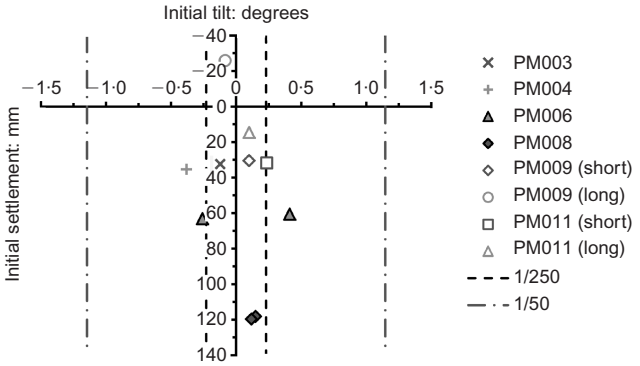

Fig. 4. Initial conditions of model structures (settlement and rotation) measured following centrifuge spin-up to 50*g* and prior to earthquake shaking

was band-pass filtered between 0·8 Hz and 8 Hz (40–400 Hz at model scale) using a zero-phase-shift digital filter to remove components of the signal that were outside the range that can be accurately controlled by the EQS. The time history of this demand motion, normalised by peak acceleration, is shown in Fig. 5(a). The Kobe earthquake was known to be particularly damaging to infrastructure, and the motion selected has a number of repetitive acceleration peaks close to the peak ground acceleration (a_g), for example, between 9 and 14 s in Fig. 5(a). In each test a $0{\cdot}1\boldsymbol{g}$ motion was initially applied to the model to characterise the dynamic behaviour of the system when the soil strains were small (negligible permanent settlement and rotation occurred during these motions). Subsequently, three nominally identical $0{\cdot}5\boldsymbol{g}$ motions were applied, representing a strong earthquake and two strong aftershocks. The initial $0{\cdot}1\boldsymbol{g}$ motion could also be

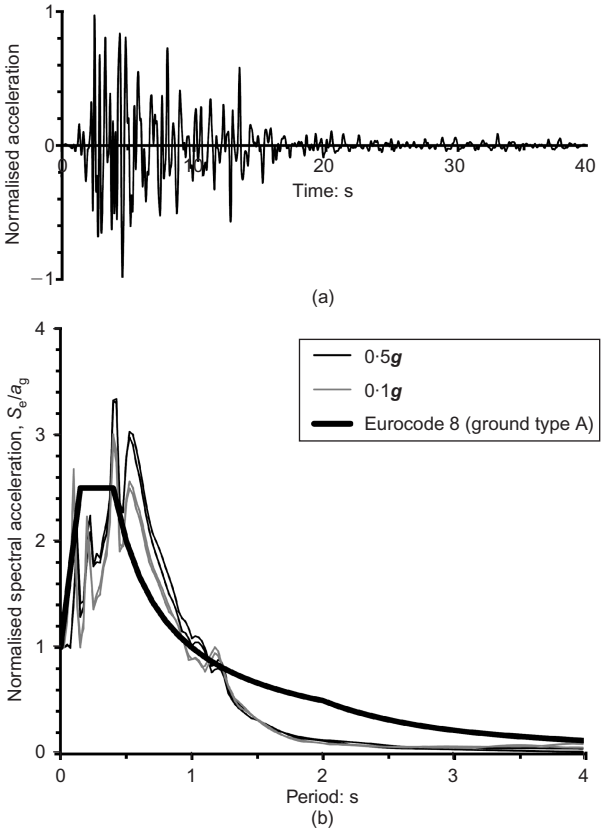

Fig. 5. Input ground notion from Nishi-Akashi recording station (Kobe in 1995): (a) normalised time history; (b) response spectra for nominal 5% damping

considered as a small pre-shock prior to the 0·5***g*** main shock. A final 0·1***g*** motion was then applied to provide a re-characterisation of the behaviour at smaller strains following the substantial changes imparted to the soil fabric by the preceding motions. The use of the same underlying record to represent all ground motions applied was an idealisation of the earthquakes being generated by the same source (and therefore having similar characteristics). The repeatability of the motions is demonstrated in Fig. 5(b) in terms of the nominal 5% damped response spectrum of the actual recorded motion at point E in Fig. 3, normalised by a_g (12 0·5***g*** motions and four 0·1***g*** motions are shown). As this represents the 'bedrock' input motion, the design spectrum from Eurocode 8 for such material (ground type A) is also shown in Fig. 5(b) for context (BSI, 2005).

FINITE-ELEMENT MODELLING

As the centrifuge model structures and foundations were long in the direction perpendicular to shaking, finite-element simulations of all of the tests were conducted in plane strain using Plaxis 2D 2012. Compared to the centrifuge model shown in Fig. 3, the dimensions of the model domain were extended laterally to 100 m and combined with non-reflecting boundary elements controlling the dynamic stresses along the vertical boundaries (after Lysmer & Kuhlmeyer, 1969) to represent semi-infinite soil conditions; that is, boundary deformations at the location of the centrifuge container wall which are controlled by the dynamic deformation of the adjacent soil. This boundary condition can also be modelled by horizontal node-to-node ties between the two vertical boundaries of a model the width of the soil tested in the centrifuge. Compared to this alternative, the method used has a higher element requirement for the same mesh density, but allowed future extension of the model beyond the two structures considered here (although the extended results are not reported in this paper). This same approach has been used previously in modelling the behaviour of slopes during a sequence of strong aftershocks in the same soil and model container, as described by Al-Defae *et al.* (2013).

The equivalent mass and vertical plates of the structures were modelled numerically using elastic plate elements having the same bending stiffness per metre length and mass as the centrifuge models (Table 1). The footings were modelled as an elastic continuum with Young's modulus of 210 GPa, Poisson ratio of 0·3 and unit weight of 76·5 kN/m^3 to match the properties of the steel footings in the centrifuge tests. Damping in each structure was modelled using Rayleigh's approach to determine the equivalent viscous damping (ς)

$$\varsigma = c_m\left(\frac{1}{4\pi f_n}\right) + c_k(\pi f_n) \tag{4}$$

where f_n are natural frequencies (of the structures). The mass- and stiffness-proportional coefficients were found by fitting equation (4) to measured damping of the model structures determined using the logarithmic decrement method applied to impulse test data, and simultaneously ensuring that the relationship is relatively flat across the full range of input motion frequencies. This is shown in Fig. 6, where mean values are shown, along with error bars representing the maximum and minimum range of the experimental impulse test data. From this figure, $c_m = 0{\cdot}4$ and $c_k = 0{\cdot}001$ were selected for use in both structures. It should also be noted that both models represent the damping of typical steel structures (~2%) well, in addition to the natural period matching shown in Fig. 2.

The soil was modelled using the 'Hardening soil model with small-strain stiffness' (Benz, 2006). This soil model

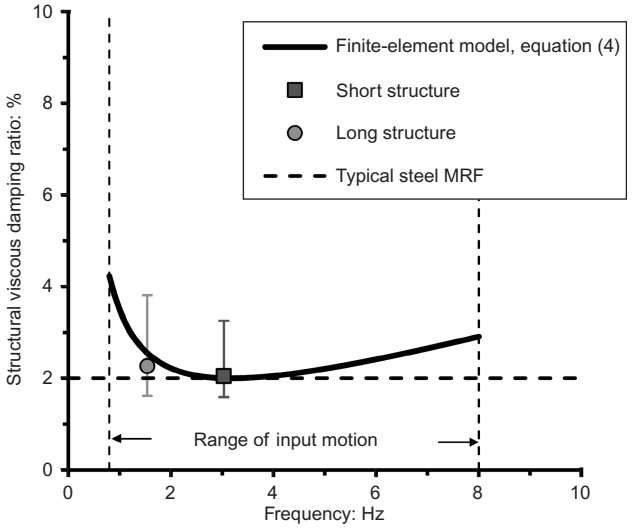

Fig. 6. Modelling of structural damping in finite-element simulations

incorporates non-linear elastic behaviour which is dependent on both confining stress level and induced strain, with Mohr–Coulomb plasticity having isotropic hardening. To examine the influence of soil parameter correlations, two different sets of parameters were used in simulations of the centrifuge tests. The first, by Brinkgreve *et al.* (2010), is non-soil specific, having been developed based on fitting to a database of historical element test data for different sands. This only requires relative density as an input parameter from which all of the constitutive parameters are obtained, potentially allowing for complete parameterisation from routine in-situ tests that can be used to estimate relative density, such as the standard penetration test (SPT) or cone penetration test (CPT) if further laboratory testing data were not available. The second set of parameters used was specifically calibrated for the HST95 sand used in the centrifuge tests through additional (routine) soil element testing, including direct shear tests and oedometric compression tests of the sand across a wide range of relative densities. A complete description of this set of parameters and the methods used to find them is given in Al-Defae *et al.* (2013). This second set of parameters also uses relative density as the input parameter. A summary of both sets of correlations is provided in Table 4. For the simulation of a particular centrifuge test, the actual relative density from Table 2 was used to obtain the constitutive parameters. Previous finite-element modelling of the behaviour of the test soil at a similar density in the same ESB container at 50***g*** by Al-Defae *et al.* (2013) has shown that some additional Rayleigh damping was required in addition to the implicit hysteretic damping included in the constitutive model, to control higher frequency components of the deformation and replicate dynamic accelerations accurately within the soil. Therefore, the same mass- and stiffness-proportional Rayleigh parameters from this previous study were used for the soil in all simulations presented here, namely, $c_m = 0{\cdot}0005$ and $c_k = 0{\cdot}005$.

Simulations using the Brinkgreve *et al.* (2010) correlations represent those that could be achieved without doing an extensive amount of site investigation; those using the Al-Defae *et al.* (2013) correlations would potentially allow improved predictions at the cost of performing an additional soil-specific calibration. Their comparison later in the paper will demonstrate how important such a calibration is to the accurate prediction of the dynamic soil and structural response. In each case, the simulations were conducted in two

Table 4. Constitutive model parameters for finite-element modelling

Parameter	Brinkgreve *et al.* (2010)	HST 95 (Al-Defae *et al.*, 2013)	Units
ϕ'_p	$12{\cdot}5D_r + 28$	$20D_r + 29$	degrees
c'	0	0	kPa
ψ'	$12{\cdot}5D_r - 2$	$25D_r - 4$	degrees
E_{oed}^{ref}	$60D_r$	$25D_r + 20{\cdot}22$	MPa
E_{50}^{ref}	E_{oed}^{ref}	$1{\cdot}25E_{oed}^{ref}$	MPa
E_{ur}^{ref}	$3E_{oed}^{ref}$	$3E_{oed}^{ref}$	MPa
ν_{ur}	0·2	0·2	–
G_0^{ref}	$68D_r + 60{\cdot}00$	$50D_r + 88{\cdot}80$	MPa
$\varepsilon_{s,0{\cdot}7}$	$2 - D_r(\times 10^{-4})$	$1{\cdot}7D_r + 0{\cdot}67(\times 10^{-4})$	–
R_f	$1 - 0{\cdot}13D_r$	0·9	–
m	$0{\cdot}7 - 0{\cdot}31D_r$	$0{\cdot}6 - 0{\cdot}1D_r$	–
γ	$4D_r + 15{\cdot}0$	$3D_r + 14{\cdot}5$	kN/m^3

Note: All reference stiffness parameters (indicated by superscript 'ref') are defined at $p' = 100$ kPa; the hardening soil model subsequently adjusts the stiffness as the confining stress changes within the continuum.

stages: Following initial stress generation to K_0 conditions (where $K_0 = 1 - \sin\phi'_p$), the structure is 'built' during a static stage; that is, the weight of the structure(s) is used to load the soil, obtain the initial stress and deformation fields within the model and achieve static equilibrium. Once this is complete the second stage applies a dynamic input motion to the bottom of the model, in each case matching that recorded in the corresponding centrifuge test. The motions were input as ground displacement histories, determined by high-pass filtering and integration of the accelerometer records; filtering before integration to obtain velocity, and again, before integrating velocity to obtain displacement ensured that there was no permanent 'wander' due to any offset in the accelerometer recordings or integration of random noise within the signal. Dynamic displacement data were then obtained at points in the finite-element model which matched those in the centrifuge tests, as shown in Fig. 7 (compare to Fig. 3). Where acceleration data were required, these were obtained by numerically double differentiating the appropriate displacement–time history.

For each of the simulations using the different parameter sets, the initial conditions were first determined direct from the initial static stage – this represents 'ideal' soil conditions. These were not the same as those in the centrifuge tests (Fig. 4), as it was impossible to achieve perfectly level placement of the structures and avoid small variations in soil properties in preparing the real soil. As the rotational behaviour is likely to be highly influenced by any initial bias in the system, a third set of simulations was also conducted, using the HST95 parameter set, but with additional vertical point loads applied to the foundation (points B, C, H and I) during the initial static step to generate a couple which forces the structure to have the initial rotations shown in Fig. 4. Such a couple, superimposed on the initially equally divided vertical loads, simulates the difference in vertical loads between footings induced by the resultant static moment on the structure that is consistent with the measured structural rotation. The magnitude and direction of the couple in each case were determined by trial and error within the initial static step of the corresponding finite-element model, so the resulting static moment and rotation are consistent with the non-linear behaviour of the foundation soil. By adding a couple, the average bearing pressure across the whole structure is unchanged (it has consistent mass), despite the loads on the different footings being distributed differently. This third set of simulations will demonstrate the importance of knowing the initial conditions of a structure prior to an earthquake (such as could be measured by surveying).

An example of the sensitivity of the rotation of isolated structures to initial conditions is shown in Fig. 8, where the three large earthquakes for test PM004 are shown, along with the input and free-field surface time histories of ground acceleration. It can be seen that if the initial rotation is matched, the finite-element model produces a very good prediction of the development of rotation throughout the first large shock and the subsequent large aftershocks. The predicted rotations are completely different using the idealised initial rotation condition. This sensitivity is exacerbated when adjacent structures are considered. Fig. 9 shows a comparison similar to Fig. 8 but for test PM006. In this particular case, the rotation of the right-hand structure is matched well in the first motion, but the left-hand structure is not (likely due to a local heterogeneity in this particular centrifuge test). As soon as the rotations begin to deviate from the centrifuge result, the match in subsequent strong aftershocks cannot be good, as the initial conditions in the subsequent earthquakes will be different. This does not imply that the finite-element model is wrong per se, just that the assumption of a uniform deposit of soil cannot model the highly subtle variations in the real soil of the centrifuge test, and that the rotation behaviour is highly sensitive to this. This is discussed further in the next section.

VALIDATION OF FINITE-ELEMENT MODEL AGAINST CENTRIFUGE TEST DATABASE

As there is a substantial amount of test data (seven tests, each having five earthquakes' worth of data), the performance of the finite-element model and effects of both material properties and initial conditions are here summarised in terms of the following key performance indicators: (*a*) peak ground acceleration near the soil surface in the free-field (point F); (*b*) peak ground acceleration at point G (in the case of adjacent structure models); (*c*) peak cyclic drift across the superstructure (between the foundation and the mass plates) in each earthquake; (*d*) post-earthquake settlement and (*e*) post-earthquake structural tilt (global rotation). It should be noted that (*c*) is a measure of super-structural demand, whereas (*d*) and (*e*) are measures of foundation performance which may affect the post-earthquake serviceability of the structure.

Figure 10(a) shows the soil amplification factor in the free field (S_{FF}) from the centrifuge tests and Fig. 10(b) presents the performance of the numerical simulations in replicating this parameter using the different sets of material parameters. The factor S_{FF} is the ratio of the peak ground acceleration at point F divided by that at point E, and the

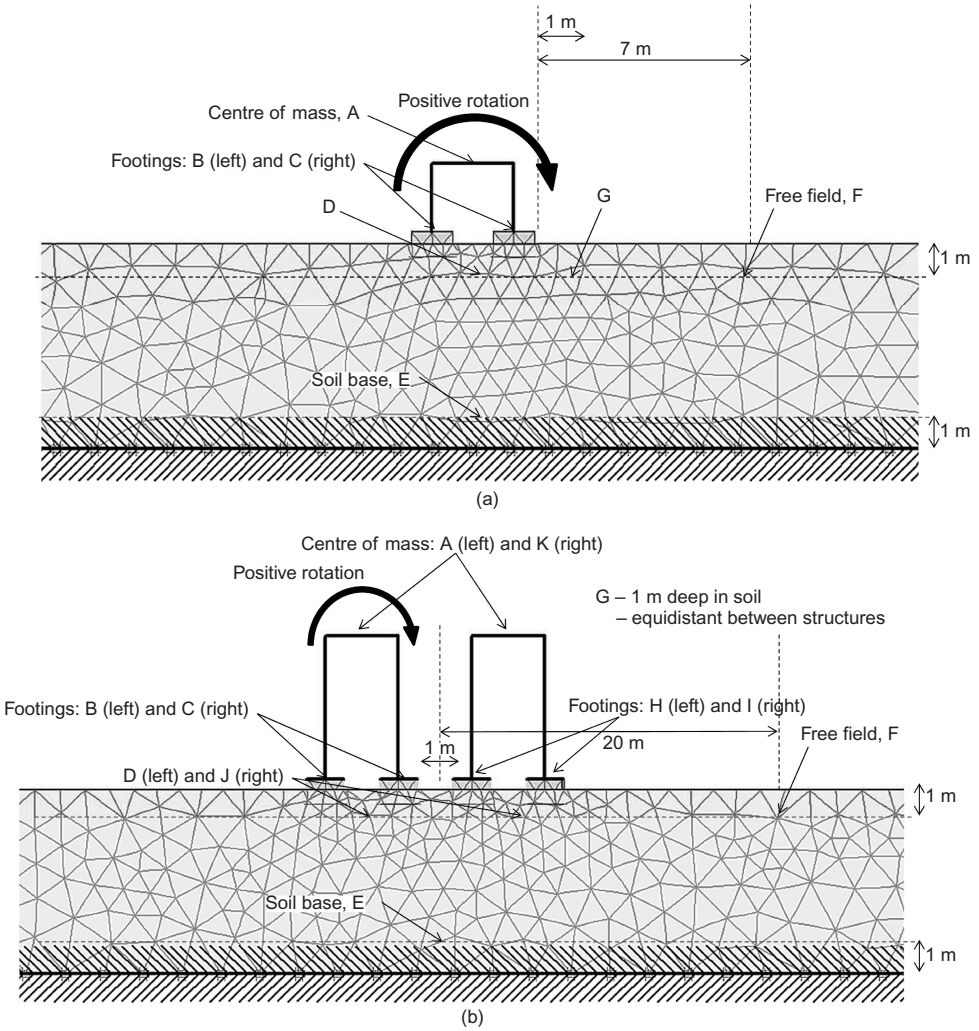

Fig. 7. Example layouts and finite-element mesh for numerical simulations: (a) PM003; (b) PM006. All dimensions at prototype scale

value of 1·4 suggested by Eurocode 8 for ground type E is also shown for context (BSI, 2005). Examples of the amplification in the time histories of motion can be seen in Fig. 8(b) and Fig. 9(c). Only the cases with ideal initial conditions are shown for the finite-element model data, as the initial conditions were not found to affect this parameter. Generally, both sets of material parameter correlations produce similar predictions of the centrifuge data, including the observation from the centrifuge that the amplification is generally larger in the smaller earthquakes. There is also a noticeable increase in S_{FF} in the smaller earthquake following the strong aftershock sequence in Fig. 10(a), presumably as a result of soil densification and a resulting stiffening of the soil response. The amplification factors are generally lower in the higher strength earthquakes as there is increasing soil inelasticity, which limits the transfer of cyclic shear stress. (Ultimately shear decoupling may occur if the ratio $(S \times a_g/\boldsymbol{g})$ becomes equal to $\tan \phi'_p$; that is, the cyclic shear stresses become equal to the shear strength of the soil. This does not happen here as the peak friction angle of the soil would require $S = 1{\cdot}68$ for $a_g = 0{\cdot}5\boldsymbol{g}$ in the free field and none of the measured values for this strength of input motion is this high in Fig. 10(a).)

Figure 11 shows the changes to the soil amplification in the near field of the structures (only data for the adjacent structure models are shown). S_{NF} is the ratio of the peak ground acceleration at point G divided by that at point E. The centrifuge data in Fig. 11(a) show, in general, a slight attenuation of ground motion close to (between) the adjacent structures. In the two finite-element cases using the ideal initial conditions (Fig. 11(b)), this behaviour is not well represented, showing instead a predominance towards amplification in the near field. When the initial conditions are correctly replicated, this tendency is reduced and a better match to the centrifuge data is obtained. This may suggest that the non-symmetrical changes to the stress distribution beneath the structures induced by the non-uniform load distribution between the footings increases the asymmetry in the interactions between the incident and reflected waves beneath the structures, encouraging destructive interference as these waves are superimposed.

Figure 12 compares the magnitude of peak drift recorded for each structure in each earthquake. These are clustered into a group of smaller values, representing the response of the short structures, and a larger set for the long structures. The variation in the magnitude of the drift is partially associated with the actual achieved strength of the input motion, variations in soil amplification in each test (e.g. Fig. 10) and SSSI. Fig. 12 suggests that the dynamic response is best simulated when the initial conditions are correctly simulated, with the idealised cases leading to an under-prediction of super-structural response.

Figure 13 shows the post-earthquake structural settlements. These are over-predicted by the Brinkgreve *et al.* (2010) set of material parameters, and under-predicted using the soil-specific HST95 parameters. The over-prediction

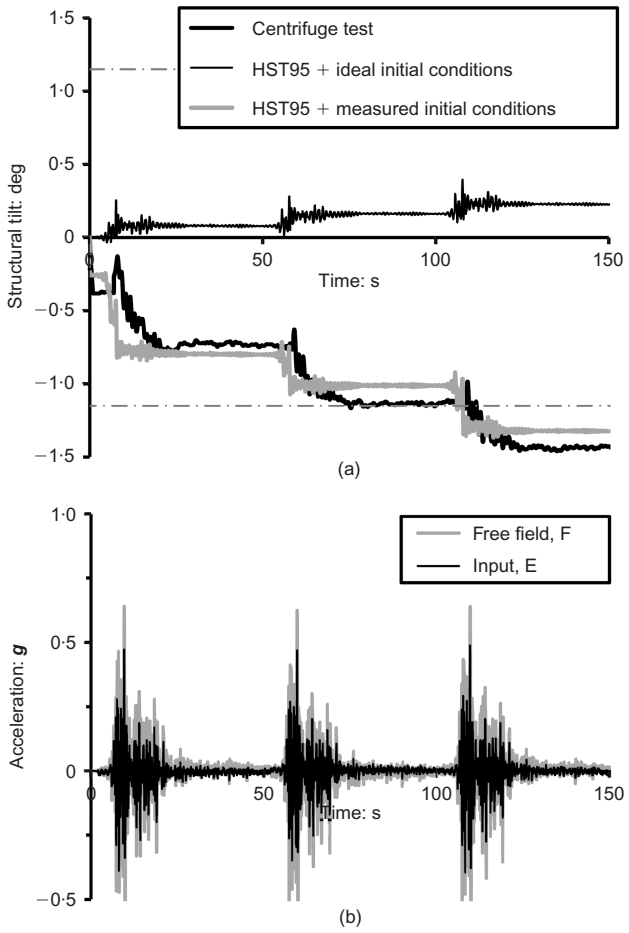

Fig. 8. Effect of initial conditions on simulated rotational response of an isolated structure during a sequence of strong earthquakes (data for PM004 shown): (a) rotations; (b) ground motions at bedrock (E) and free field (F) (as recorded in the centrifuge)

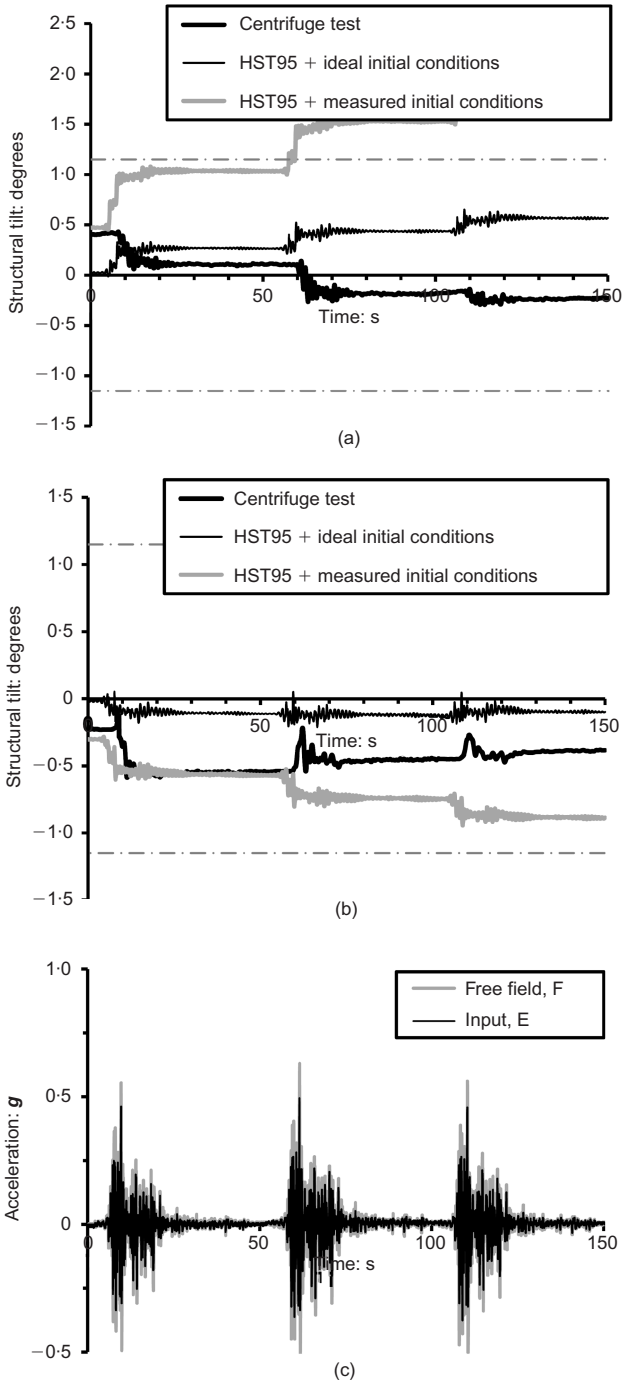

Fig. 9. Effect of initial conditions on simulated rotational response of adjacent identical structures during a sequence of strong earthquakes (data for PM006 shown): (a) rotation of left structure; (b) rotation of right structure; (c) ground motions at bedrock (E) and free field (F) (as recorded in the centrifuge)

within the former is likely to be attributable to the lower soil strength (peak friction angle – see Table 4) meaning that soil yield occurs earlier and greater settlements are accrued. The Brinkgreve *et al.* (2010) set of parameters was similarly found by Al-Defae *et al.* (2013) to over-predict permanent seismic slope deformations in the same sand (at a similar relative density). These observations demonstrate the benefits of investing additional effort and resources in performing a soil-specific model calibration on accurate prediction of permanent deformations. The importance of correct simulation of the initial conditions is also highlighted, as for peak drift. Using the idealised initial conditions resulted in a starting position with comparative amounts of settlement of each foundation (low initial rotation). Applying the couple to generate the measured initial conditions generally resulted in an increase in the load on one of the foundations, while reducing it on the other. As the soil response is non-linear, the foundation under greater compressive loading will be pushed into a more inelastic part of the load–settlement curve, resulting in greater settlements. This would be expected in the centrifuge too, assuming that the stress distribution is similarly altered as a result of the measured initial conditions. As settlement of the structure is the average of the settlements of the two foundations, this may explain the lower settlements for the idealised initial conditions compared to both the case with measured initial conditions and the centrifuge data, which match well.

Figure 14 compares the post-earthquake permanent rotations (tilts) of the structures. Fig. 14(a) includes all of the data, and shows a number of significant outliers, particularly along the x-axis (i.e. the finite-element model is predicting large rotations). These points are associated with the later earthquake motions of the adjacent structure tests when substantial permanent rotations had accrued in the finite-element model owing to the successive strong shaking, and are to be expected given the example results from Fig. 9. In Fig. 14(b), only the data from the first 0·1$\boldsymbol{g}$ and first 0·5$\boldsymbol{g}$ motions are plotted, which results in a strong positive correlation, but only when the initial conditions are correctly modelled. This also serves to highlight the data for the two sets of simulations which used idealised conditions, where it

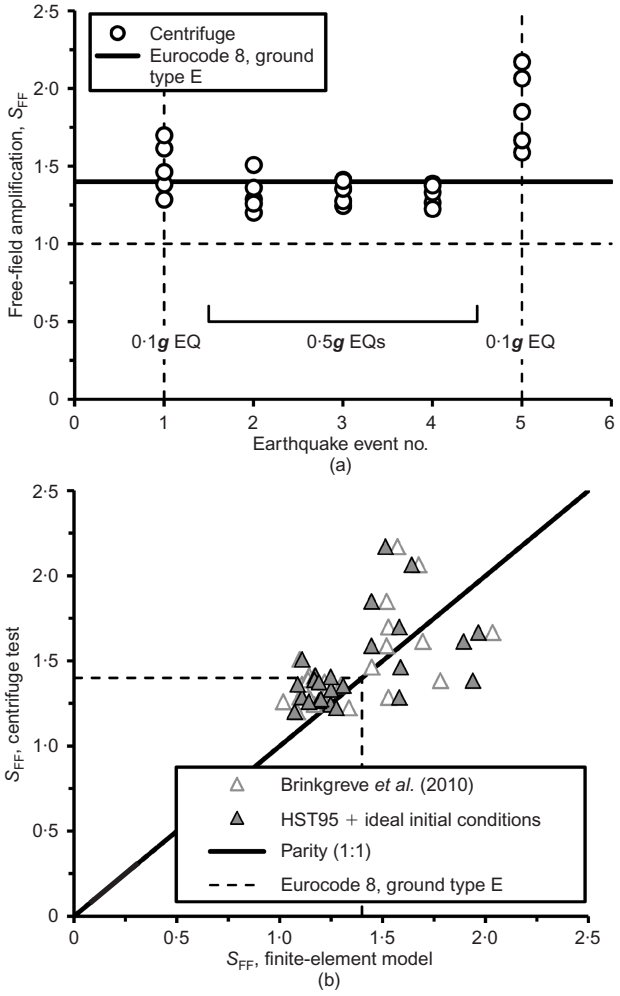

Fig. 10. Effect of soil material parameter correlations on prediction of site effect in the free field through a sequence of strong earthquakes: (a) centrifuge data, adjacent structure tests; (b) comparison of finite-element method predicted values to centrifuge data

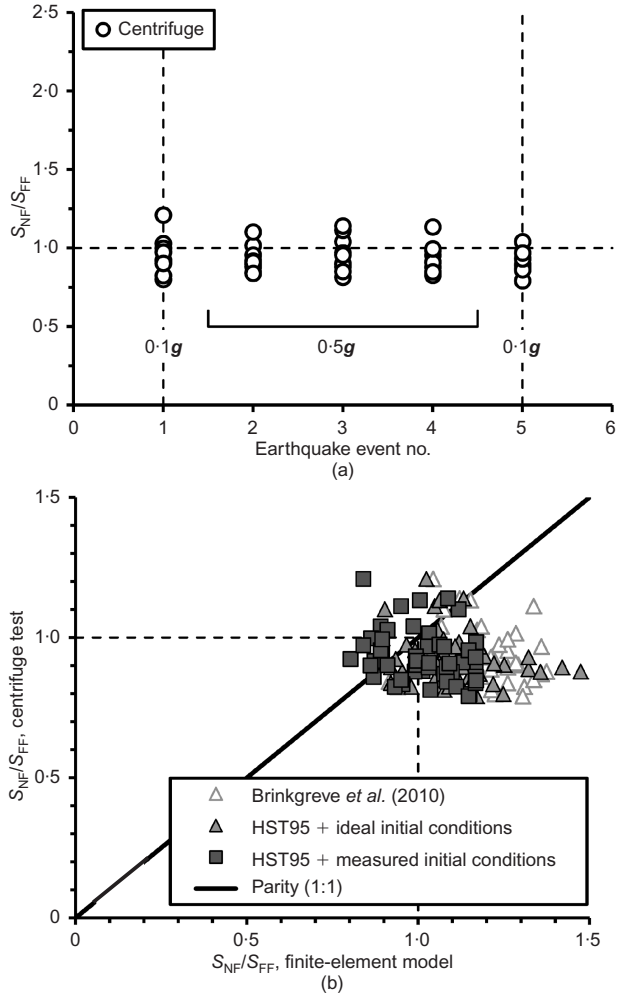

Fig. 11. Effect of soil material parameter correlations and structural initial conditions on amplification/attenuation of ground motion in the near field (point (G), adjacent structure cases): (a) centrifuge data; (b) comparison of finite-element method predicted values to centrifuge data

can be seen that neither set of material properties provides any correlation with the centrifuge results.

Validation summary

Linear relationships were fitted to the individual data sets in Figs 10(b), 11(b), 12, 13 and 14(b) (and also for data of S_{NF} plotted as centrifuge against finite-element model), using a least-squares fitting procedure. The gradient of these relationships demonstrates, on average across the full dataset, the degree of over- or under-prediction. The inverse of these gradients, plotted as percentages, are summarised in Fig. 15 for the performance indicators (*a*)–(*e*). This shows that in order to achieve the best simulation of soil structure interaction and SSSI (at least for pairs of structures), it is necessary to both obtain a soil-specific set of model parameters (as also concluded by Al-Defae *et al.* (2013)) and to model the actual initial (rotation) conditions of the structure(s). When applied in practice to field structures, this could be measured based on structural surveying of the building stock, and would need to be updated if this varied with time since construction. When both material properties and initial conditions are correctly modelled, all five of the performance indicators can generally be predicted within ±10% averaged error across the 35 different earthquake and structure combinations considered in this paper, although

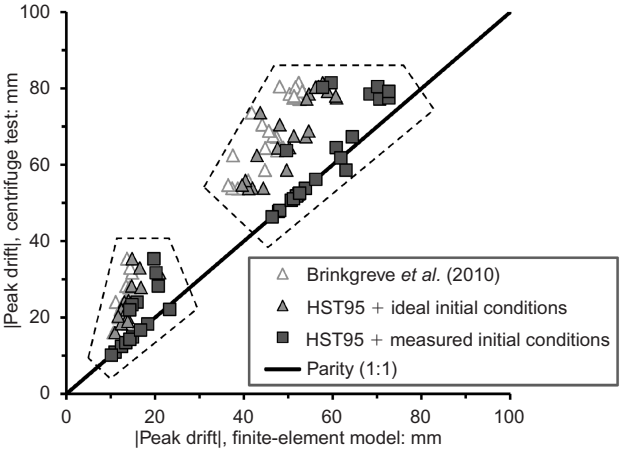

Fig. 12. Effect of finite-element method modelling assumptions on estimation of peak drift

there are some outlying points, which are perhaps to be expected given the extensive amount of earthquake shaking applied to each model, and therefore the potential for small differences to become amplified by the end of the earthquake sequence.

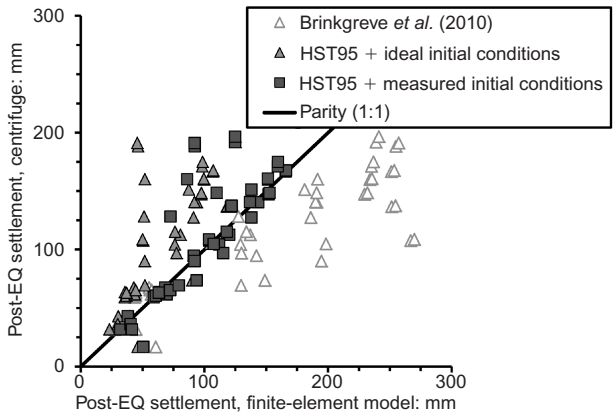

Fig. 13. Effect of finite-element method modelling assumptions on estimation of post-earthquake settlement

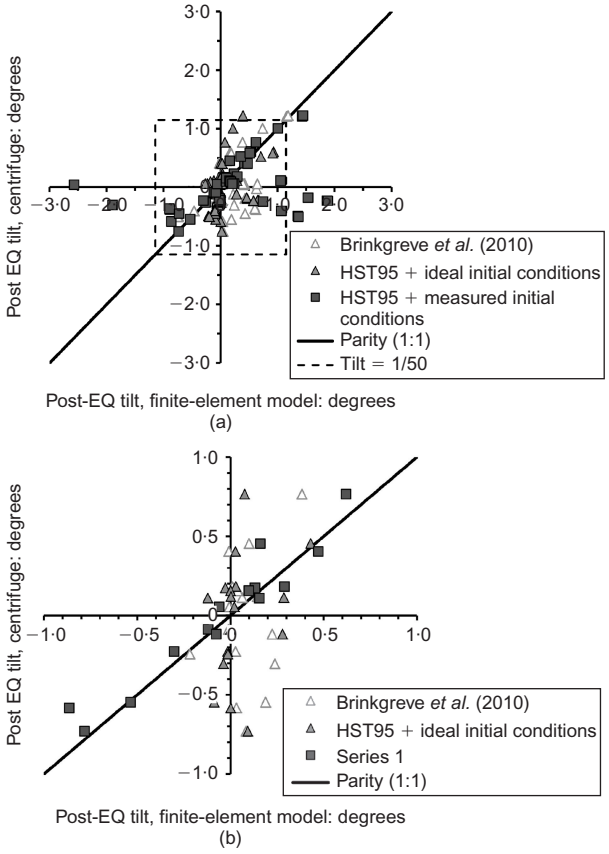

Fig. 14. Effect of finite-element method modelling assumptions on estimation of post-earthquake permanent rotation (structural tilt): (a) all earthquakes; (b) earthquakes EQ1 (first 0·1*g* motion) and EQ2 (first 0·5*g* motion) only

INSIGHTS INTO SSSI OF PAIRS OF ADJACENT STRUCTURES

Although the centrifuge test data are valuable as a means of validating the finite-element model and understanding the importance of the modelling assumptions (material properties and initial conditions), direct comparison across tests, particularly in terms of settlement and tilt, is not ideal, owing to the different initial conditions in the tests (Fig. 4). The rotation behaviour has also been shown to be highly sensitive to the exact ground conditions which match well, but not perfectly across the different centrifuge models (relative density in Table 2). The finite-element method, however, presents an opportunity to compare model behaviour

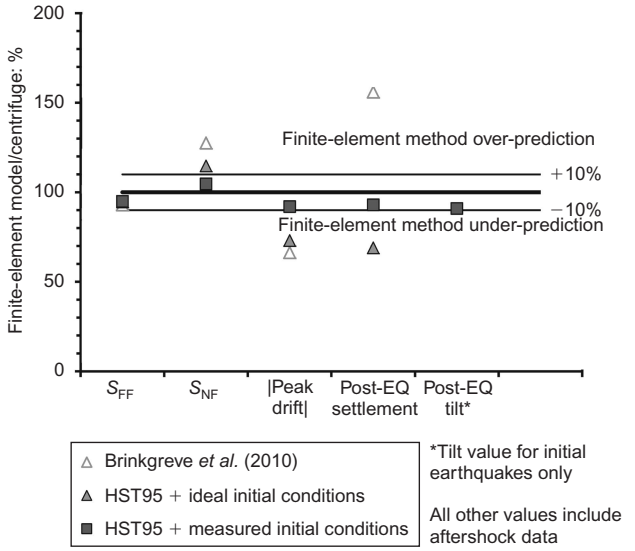

Fig. 15. Summary of finite-element method validation against centrifuge test data

for perfectly ideal and identical ground. In this section, finite-element analyses using the HST95 material model and ideal initial conditions are therefore compared to demonstrate the effects of the presence of an adjacent structure on the resulting SSSI and structural response, all other conditions being equal, using the same Kobe earthquake motion and order of consecutive motions as described previously.

The results are summarised in Figs 16–18 and will be discussed together at the end of the section. Fig. 16 shows the peak drifts normalised by those of the isolated structures. The data are separated by earthquake strength and by structure type, and each data point represents an average across the different motions; for example, for the case of similar tall structures, the 0·5***g*** point in Fig. 16 is the average of the EQ2, EQ3 and EQ4 responses for both structures. Fig. 17(a) shows a comparison of the permanent movements (settlement and tilt) of a long structure when it is either on its own (‘isolated’), adjacent to an identical structure (‘Similar’, with ‘L’ and ‘R’ denoting left and right

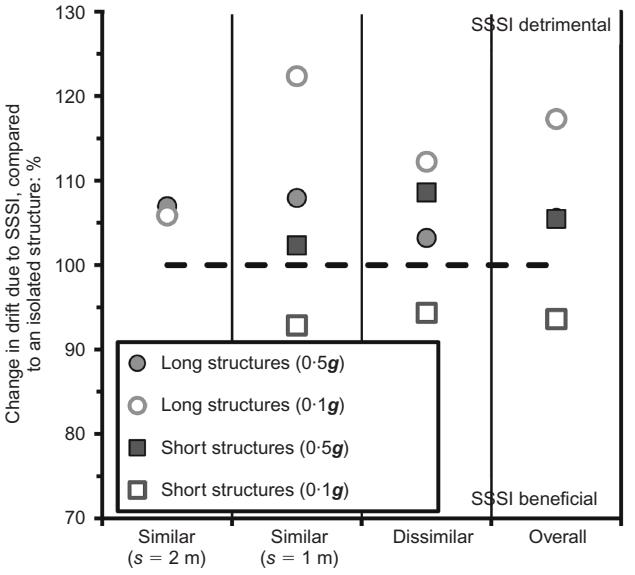

Fig. 16. Summary of effect of adjacent structure properties and earthquake strength on drift amplification/attenuation due to SSSI (ideal initial conditions)

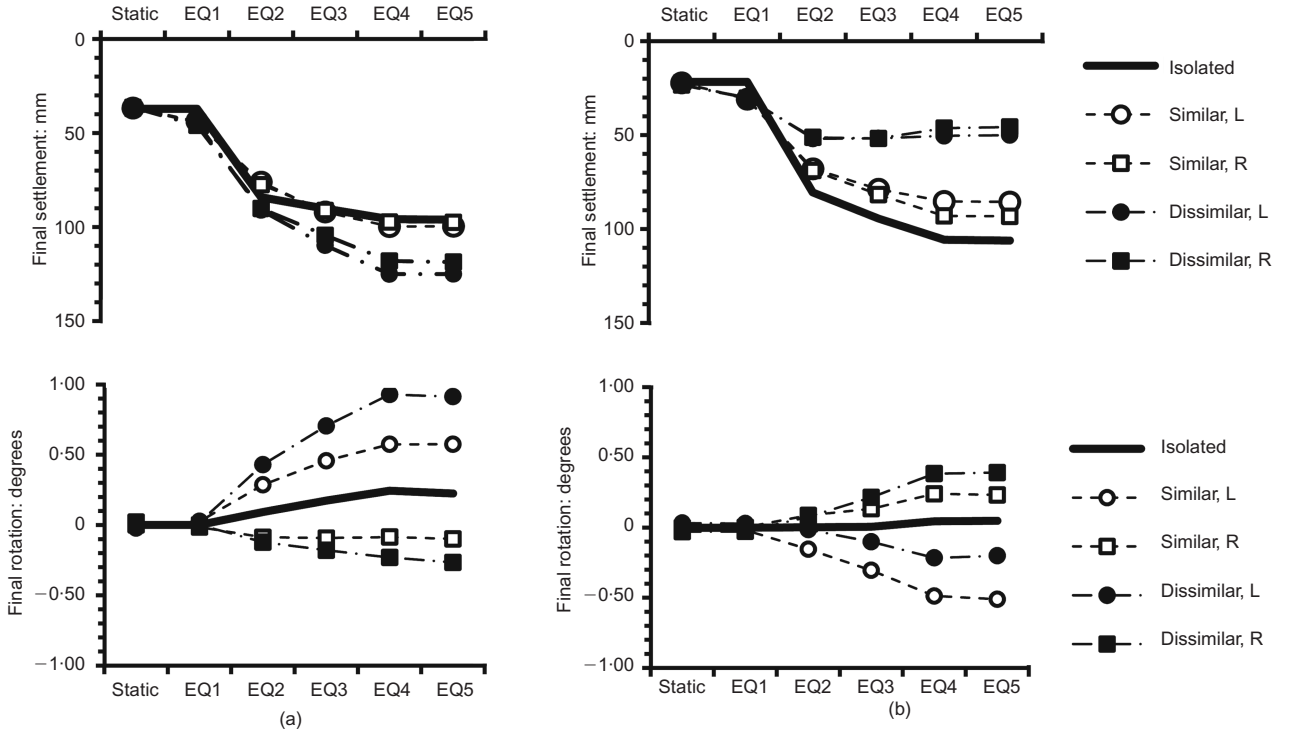

Fig. 17. Effect of adjacent structure properties, earthquake strength and strong aftershocks on development of settlement and tilt due to SSSI (ideal initial conditions): (a) long structures; (b) short structures

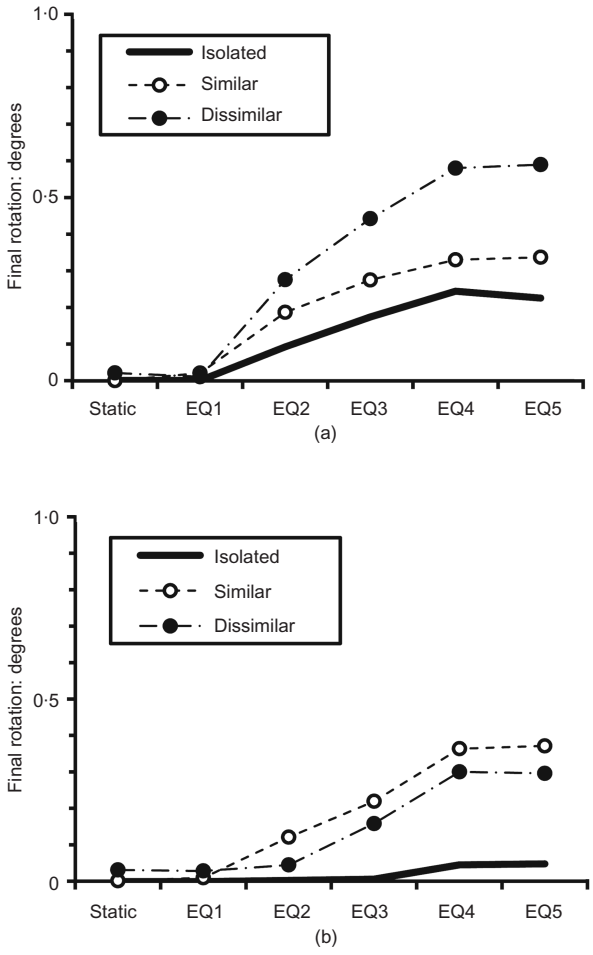

Fig. 18. Magnitude of structural tilt (average of both earthquake directions): (a) long structures; (b) short structures

of the pair relative to the direction of the earthquake and the geometry shown in Fig. 7), or next to a smaller structure ('Dissimilar'). Fig. 17(b) shows similar data for a short structure when it is isolated, next to an identical structure, or next to a larger structure. As the rotation may be different depending on whether the structure is on the left or right of the arrangement (this essentially represents the earthquake motions being in opposite directions), Fig. 18 shows the average of the absolute rotations of the 'L' and 'R' cases from Fig. 17. Based on Figs 16–18, the following insights can be drawn.

(*a*) Insights for the case where a structure is situated next to an identical neighbour.
  (*i*) The drift may or may not be increased, depending on the natural period of the structure in question and the strength of the earthquake. In this study, in small earthquakes inducing a smaller strain soil response, SSSI increased drift for long period structures and reduced it for short period structures; in larger earthquakes with a strong elasto-plastic near-field response, SSSI increased drift for both types of structure by between 2 and 10% (Fig. 16).
  (*ii*) The settlement is either unaffected, or slightly reduced due to the adjacent structure providing additional confinement to the soil beneath the foundations (Fig. 17).
  (*iii*) The magnitude of the rotation of the structure increases (Fig. 18), and it rotates away from its neighbour (compare hollow circle and hollow square markers in Fig. 17(a) or Fig. 17(b); the sign convention is shown in Fig. 7). This outward ratcheting is thought to occur as plastic soil deformation is confined by the adjacent structure while the structure is rotating towards its neighbour, whereas soil deformation while rotating outwards (away from its neighbour) is not. This means that

there would be a net rotation outwards in a given cycle of deformation, which would then progressively accrue in subsequent cycles due to P–Δ effects.

(*b*) Insights for the case where a structure is situated next to a shorter neighbour (having lower natural period and bearing pressure).
   (*i*) SSSI increases drift compared to the isolated case, but by less than when the neighbouring structure is identical, and in both small and large earthquakes (Fig. 16).
   (*ii*) The settlement is increased (Fig. 17(a)).
   (*iii*) The magnitude of rotation of the structure increases, by more than when the neighbouring structure is identical (Fig. 18(a)). It rotates towards its neighbour (positive rotation if on the left of the pair and negative rotation if on the right, Fig. 17(a)).

(*c*) Insights for the case where a structure is situated next to a taller neighbour (having higher natural period and bearing pressure).
   (*i*) SSSI appears to increase drift in larger earthquakes but reduce it in smaller earthquakes compared to the isolated case. Irrespective of earthquake strength, however, drift is larger than the case when the neighbouring structure is identical (Fig. 16).
   (*ii*) Settlement is reduced (Fig. 17(b)).
   (*iii*) The magnitude of rotation of the structure increases, by less than when the neighbouring structure is identical (Fig. 18(b)). It rotates away from its neighbour (negative rotation if on the left of the pair and positive rotation if on the right, Fig. 17(b)).

These conclusions should not be considered to be general, as there is a need to perform further simulations with different types of structure (particularly to investigate the effect of different building widths and foundation types) and on different types of ground to demonstrate generality. However, they do demonstrate that the presence nearby of even a single adjacent structure can have a dramatic effect on a structure's seismic response compared to a consideration of the same structure and underlying ground in isolation. These effects appear to be either beneficial or detrimental, depending on the relative dynamic properties of the adjacent structures and strength of the earthquake (i.e. soil response). This suggests that through further study it may be possible to exploit the beneficial effects of SSSI and avoid the detrimental ones to improve the seismic performance of the built environment.

CONCLUSIONS

This paper has examined how the performance of a simple structure is altered when it is situated close to an adjacent structure, as a first step towards a better understanding of the seismic response of densely packed urban areas. Dynamic centrifuge modelling was conducted such that the full non-linear behaviour of the soil could be incorporated into the SSSI. This generated a database of performance data against which non-linear finite-element models were validated. The importance of both generalised or soil-specific material properties and the initial geometric configuration of the structure (initial conditions) was investigated, and it was demonstrated that accurate simulations could be achieved so long as soil-specific material properties can be determined and the initial conditions are known. (This would require building surveys for field application and laboratory testing of soils to generate site-specific soil property calibrations.) The finite-element approach was subsequently used to investigate the effects of the presence of an adjacent structure of either similar or dissimilar type. This demonstrated that the structural drift and co-seismic settlement could be reduced or increased as a result of SSSI, depending chiefly on the properties of the adjacent structure (building height was considered here, in terms of changes to the fundamental period and foundation bearing pressure). This suggests that, through further study, it may be possible in the future to prescribe dynamic properties in seismic design to exploit beneficial effects of SSSI with the surrounding urban environment. However, in all cases, permanent rotation (tilt) of the structure was observed to increase compared to the isolated case as a result of SSSI, and so consideration must also be given to effective ways of remediating this.

ACKNOWLEDGEMENTS

This work was supported by the Engineering and Physical Sciences Research Council (EPSRC) under grant no. EP/H039716/1, which the authors acknowledge with thanks. The authors would additionally like to express their sincere gratitude to Mark Truswell and Colin Stark at the University of Dundee for their assistance in performing the centrifuge tests.

NOTATION

a_g	peak ground acceleration at bedrock/input
B	footing width (in plane of shaking)
C_t	empirical period determination factor
C_u	coefficient of uniformity
C_z	coefficient of curvature
c_k	stiffness-proportional Rayleigh damping coefficient
c_m	mass-proportional Rayleigh damping coefficient
c'	cohesion intercept
D_r	relative density
D_{10}	particle diameter at which 10% is smaller
D_{30}	particle diameter at which 30% is smaller
D_{60}	particle diameter at which 60% is smaller
E_{oed}	oedometric tangent stiffness (in compression)
E_{ur}	unloading–reloading stiffness
E_{50}	triaxial secant stiffness (at 50% of deviatoric failure stress in drained triaxial compression)
EI	elastic bending stiffness
e_{max}	maximum void ratio
e_{min}	minimum void ratio
FS_v	static vertical factor of safety
f_n	natural frequency
G_s	specific gravity of soil grains
$G_{(0)}$	(small strain) shear modulus
$\boldsymbol{g}$	acceleration due to gravity ($= 9{\cdot}81$ m/s^2)
H	height
K_{eq}	equivalent lateral sway stiffness
K_0	coefficient of lateral earth pressure at rest
M_{eq}	equivalent mass
M_w	moment magnitude
m	power-law index for stress-dependency of stiffness
N_γ	footing bearing capacity factor
p'	mean effective stress
q	bearing pressure
R_f	deviatoric failure ratio
S_e	spectral acceleration
$S_{(FF,NF)}$	Eurocode 8 equivalent soil factor (free-field, near-field)
s	footing spacing (centre-to-centre)
s_γ	footing shape factor
T_{n0}	fundamental natural period
γ	soil unit weight (dry)
$\varepsilon_{s,0{\cdot}7}$	shear strain at $G/G_0 = 0{\cdot}7$
ν_{ur}	Poisson ratio (unload–reload)
ς	equivalent viscous damping
ϕ'_p	(secant) peak angle of friction
ψ'	dilation angle

REFERENCES

Al-Defae, A. H., Caucis, K. & Knappett, J. A. (2013). Aftershocks and the whole-life seismic performance of granular slopes. *Géotechnique* **63**, No. 14, 1230–1244, http://dx.doi.org/10.1680/geot.12.P.149.

Alexander, N. A., Ibraim, E. & Aldaikh, H. (2013). A simple discrete model for interaction of adjacent buildings during earthquakes. *Comput. Structs* **124**, 1–10.

Benz, T. (2006). *Small-strain stiffness of soils and its numerical consequences*. PhD thesis, University of Stuttgart, Germany.

Bertalot, D. (2012). *Behaviour of shallow foundations on layered soil deposits containing loose saturated sands during earthquakes*. PhD thesis, University of Dundee, UK.

Bertalot, D., Brennan, A. J., Knappett, J. A., Muir Wood, D. & Villalobos, F. A. (2012). Use of centrifuge modelling to improve lessons learned from earthquake case histories. *Proceedings of the 2nd European conference on physical modelling in geotechnics, Eurofuge 2012*, Delft, the Netherlands.

Betti, R. (1997). Effects of the dynamic cross-interaction in the seismic analysis of multiple embedded foundations. *Earthquake Engng Structl Dynam.* **26**, No. 10, 1005–1019.

Brennan, A. J., Knappett, J. A., Bertalot, D., Loli, M., Anastasopoulos, I. & Brown, M. J. (2014). Dynamic centrifuge modelling facilities at the University of Dundee and their application to studying seismic case histories. In *Proceedings of the 8th international conference on physical modelling in geotechnics* (eds C. Gaudin and D. J. White), pp. 227–233. London, UK: Taylor & Francis Group.

Brinkgreve, R. B. J., Engin, E. & Engin, H. K. (2010). Validation of empirical formulas to derive model parameters for sands. In *Numerical methods in geotechnical engineering* (eds T. Benz and S. Nordal). Rotterdam, the Netherlands: CRC Press/Balkema.

BSI (2004). BS EN 1997-1:2004: Eurocode 7: Geotechnical design – Part 1: General rules. British Standards Institution, London, UK.

BSI (2005). BS EN 1998-1:2005: Eurocode 8: Design of structures for earthquake resistance – Part 1: General rules, seismic actions and rules for buildings. British Standards Institution, London, UK.

Goel, R. K. & Chopra, A. K. (1997). Period formulas for moment-resisting frame buildings. *J. Structl Engng* **123**, No. 11, 1454–1461.

Lauder, K. (2011). *The performance of pipeline ploughs*. PhD thesis, University of Dundee, UK.

Lyamin, A. V., Salgado, R., Sloan, S. W. & Prezzi, M. (2007). Two- and three-dimensional bearing capacity of footings in sand. *Géotechnique* **57**, No. 8, 647–662, http://dx.doi.org/10.1680/geot.2007.57.8.647.

Lysmer, J. & Kuhlmeyer, R. L. (1969). Finite dynamic model for infinite media. *ASCE J. Engng Mech. Div.* **95**, No. 4, 859–887.

Muir Wood, D. (2004). *Geotechnical modelling*. Abingdon, Oxfordshire, UK: Spon.

Padrón, L. A., Aznárez, J. J. & Maeso, O. (2009). Dynamic structure–soil–structure interaction between nearby piled buildings under seismic excitation by BEM–FEM model. *Soil Dynamics Earthquake Engng* **29**, No. 6, 1084–1096.

Salgado, R. (2008). *The engineering of foundations*. New York, NY, USA: McGraw-Hill.

Stewart, J. P., Seed, R. B. & Fenves, G. L. (1999). Seismic soil-structure interaction in buildings, Part II: Empirical findings. *J. Geotech. Geoenviron. Engng* **125**, No. 1, 38–48.

Tsogka, C. & Wirgin, A. (2003). Simulation of seismic response in an idealized city. *Soil Dynam. Earthquake Engng* **23**, No. 5, 391–402.